NUMERICAL SIMULATION OF AIR FLOW PAST A FULL HELICOPTER CONFIGURATION

W. Khier, Deutsches Zentrum für Luft- und Raumfahrt e.V.(DLR), Braunschweig, Germany

Abstract

A detailed comparison between blind time-accurate RANS simulation of the GOAHEAD configuration and wind tunnel results is presented. The computational model refers to a wind tunnel complete helicopter model, featuring a 4.1 m NH90 fuselage model, ONERA 7AD main rotor, reduced scale BO105 tail rotor, a rotor hub, a strut and slip ring fairing inside the 8m x 6m test section of the DNW low-speed wind tunnel. The flow solver, FLOWer, was weakly coupled to the flight mechanics tool HOST to predict the elastic deformation of the main rotor blades. The flight conditions correspond to cruise flight at Ma=0.204 and fuselage attitude α=-2^o. The comparisons with the blind computations revealed broadly good to very good agreement with experiment.

1. INTRODUCTION

Proper simulation of the deformation of main rotor blades plays a decisive role for the accurate prediction of pressure and sectional loads of main rotor blades. This is due to the fact that most of main rotor blades are deformed under the aerodynamic and inertial loading. This elastic bending and twist deformations leads to change in the effective angle of attack experienced by the blade, and thus, the development of different pressure schemes on the blade, especially in the advancing range. Early attempts of the author [1] to simulate a helicopter using rigid blades assumption lead to considerable discrepancy in pressure, in line with the findings of reference [2].

For a numerical simulation process of helicopters to be meaningful, low speed flow and three dimensional separation on the fuselage, transonic and supersonic flow on the blades, as well as the interactional phenomena associated with helicopter flows have to be predicted adequately. In order to verify the fulfillment of these requirements by any CFD simulation process, an extensive validation of the applied numerical tools is needed.

Unfortunately, the vast majority of published experimental data were generated for other research objectives (Ref. [3] and [4], for example). Therefore, the EU project GOAHEAD, [5] and [6] was initiated by a consortium of leading European helicopter manufacturers and research institutes to generate a comprehensive experimental database especially conceived to validate CFD codes in helicopter related applications. The measurements were successfully carried out at the German-Dutch low speed wind tunnel (DNW) in spring 2008 [7]. The GOAHEAD test campaign included detailed steady and unsteady surface pressure measurements on the helicopter and tunnel walls, transition locations, inflow data and PIV measurements for a wide array of flight and rotor loading conditions. The blind test computations were carried out about 18 months ahead of the measurements. A description of the GOAHEAD blind test activity, its objective and outcome is given in reference [8]

In this paper a detailed comparison between CFD and experimental results of the flow past a complete helicopter model is reported. The main objective of the investigation is to assess and to evaluate the ability and accuracy of present day CFD tools to capture the flow phenomena pertinent to helicopters. The investigation presented in this paper can be regarded as a continuation of the studies reported in [9],[18] and (partially) [8]

The computational model refers to the tested GOAHEAD wind tunnel model. Owing to technical reasons, several changes in the geometry had to be introduced during the construction of the model. The numerical results were obtained via time-accurate solution of RANS equations in three dimensions using the DLR finite volume, block-structured solver FLOWer ([10] and [11]) weakly coupled to the flight/structural mechanics tool HOST [12]. Chimera overlapping grid approach was applied to introduce the motion of the blades.

The computational model and flow conditions are described in the next part. The numerical approach and computational grid are presented in the subsequent parts. The fifth part of the paper is dedicated to the numerical results and their comparison with the experimental data. Finally, the conclusions are listed in the sixth and last section of this paper.

2. COMPUTATIONAL MODEL AND FLOW CONDITIONS

The computational model refers to the GOAHEAD wind tunnel model (Figure 1). It consists of a 4.1 m NH90 fuselage model, ONERA 7AD main rotor, reduced scale BO105 tail rotor, a main rotor hub, a strut and slip ring fairing and 8m x 6m test section of 20m length. Both the main and tail rotors are represented by isolated blades. The main rotor hub is simplified to a cylindrical element and an elliptical hub fairing. The tail rotor hub is not included in the computational model.

Forward flight condition at Mach number equal 0.204 and -2.0^o fuselage pitch angle was considered. The experiment was performed however with a fuselage pitch angle of -2.5^o. These flight parameters were found associated with tail shake phenomenon by flight mechanics tools. Tail shake is a wake induced vibration problem arising from interference between the wake of main rotor hub and the tail part. The problem of tail shake involves structural and flight dynamic analysis of the fuselage, which will not be tackled in this paper.

3. APPROACH

The numerical approach employed in this paper is based on the solution of the Reynolds (Favre) averaged Navier-Stokes equations in three dimensions accurately in time by means of the CFD simulation code FLOWer. In the solution process, the mass, momentum and energy fluxes are represented by second order central differences. Third order numerical dissipation is added to the convective fluxes to ensure numerical stability. These dissipative contributions are reduced to first order when a shock is detected. Smooth transition from the third to the first order is realized by linear combination of both terms. FLOWer contains a large array of statistical turbulence models, ranging from algebraic and one-equation eddy viscosity models (Refs [12]-[14]) to seven-equation Reynolds stress model. In this paper a slightly modified version of Wilcox's two-equation k-ω model is used (Refs. [15] and [16]). Unlike the main flow equations, Roe's scheme is employed to compute the turbulent convective fluxes.

The rotor was trimmed to pre-defined weight, lateral and propulsive force coefficients using the stand alone flight mechanics tool HOST (Helicopter Overall Simulation Tool). The resulting rotor controls and elastic deformation of the blade surface for the whole radial and azimuth range were then imposed on the CFD simulation to modify the blade surface geometry following the approach presented in [17]-[20]. The process was repeated until the variation in elastic blade deformation and rotor control angles have fallen below a user defined tolerance.

4. NUMERICAL GRID

Multi-block grids around the different elements were subdivided into 10 Chimera components: fuselage, rotor hub, four main rotor blades, two tail rotor blades, model strut and wind tunnel walls. Figure 1 shows the surface grid for the complete helicopter configuration, while Table 1 lists the major characteristics of the numerical grid.

	No. of blocks	Number of points
Fuselage	90	9 500 000
Main rotor blade (x 4)	10	870 000
Tail rotor blade (x 2)	3	350 000
Rotor hub	8	900 000
Strut	12	530 000
Wind tunnel	13	300 000
Total (block/Mil. point)	169	15 400 000

Table 1: Grid parameters

5. RESULTS

The fuselage is equipped with a total number of 130 unsteady pressure sensors. Figure 3 contains a comparison between experiment and CFD for selected 13 sensors. It should be noted that the main rotor rotates in clockwise direction as seen from above. The upper vertical tail rotor blade is advancing and the lower vertical is retreating. The experimental results were recorded over 130 main rotor revolutions. The experimental data shown in the figure is merely the arithmetic mean of the recorded data. Their maxima and minima at each azimuthal position varied considerably, as shown in Figure 2. Analysis of the experimental data and its quality is beyond the scope of the current paper. However, at a first glance this strong variation in pressure seems to be caused by vibration of the wind tunnel model.

Good agreement between measurements and computations can be observed for the sensors on the nose (Figure 3.a) and on the windscreen (Figure 3.b and c). The influence of the rotor is well captured in the computations in terms of frequency and phase. Except for the nose sensor, Figure 3.a, the amplitude is predicted accurately. Discrepancies are observed for the pressure minima and evolution of the signal over the azimuth.

The pressure is shown in Figure 3.d and e for two sensors on the upper side of the tail boom. A clear 4/Rev pattern can be identified in the experiment and in the computations emphasizing the influence of the main rotor in this region. While the peak value and its location is accurately computed for sensor

(d), the corresponding values of sensor (e) are only fairly predicted. The pressure levels for the later sensor are somewhat underestimated in the computations. The computed patterns for both sensors are characterized by strong oscillations after the peaks. A similar behaviour cannot be observed in the experiment.

Figure 3.f and g depict the pressure signals of two sensors on the lower side of the tail boom. The computations overestimate the rise in pressure between the windward (f) and leeward (g) (with respect to the main rotor) sensors. Despite the discrepancies in the evolution of the signal, the azimuth locations of the four pressure peaks are predicted with reasonable accuracy. The observed deviation is likely to be due to the use of different strut fairing in the experiment. As mentioned earlier, a bluff strut fairing was originally planned to be used in the experiment. The computational geometry was based on this original configuration. However, it was decided later after the conclusion of the computations to replace the original strut fairing by a streamlined one in the experiment Figure 4 compares the designs used in the blind test phase and in the experiment.

On the leading edge of the tail fin (Figure 3.h and l), the behavior of the lower sensor signal can be interpreted as 2/Rev. CFD results shows a similar pattern but with a clear deviation from the experiment. The same cannot be observed for the upper sensor. No clear trend can be identified for both the experimental and the numerical pressure signals. Geometrical differences in the rotor mast fairing area and tail fin shape is a possible reason for the observed deviation (see
Figure **5**).

Very good match could be obtained on the windward (with respect to the main rotor) sensor of the tail fin (Figure 3.j). Both amplitude and frequency could be computed with good accuracy. However, the amplitude of the suction peaks is overestimated in the computations. The pressure signal in this area is dominated by the tail rotor as can be seen from the 10/Rev behavior observed in the measured and computed data. The leeward sensor (Figure 3.k) shows an evident deviation from the experimental data. Neither the experimental nor the numerical signals are characterized by a clear trend.

The computations predict higher pressure on the horizontal stabilizer as can be seen in Figure 3.l and m. This deviation can be also attributed to geometrical incompatibility between the computational geometry and the measured one. The horizontal stabilizer in the wind tunnel model was mounted downstream its location in the computational geometry and had a different dihedral.

Figure 3.m-p show the signals of selected three sensors in the dog house region. A departure form the experimental data can be clearly seen. The computations did not reproduce the rise in pressure observed in the direction (m) to (p). Since the sensors are mounted in the downstream vicinity of the strut, the previously mentioned influence of strut fairing geometry is a probable cause for the discrepancy.

Computed and measured pressure coefficients on the main rotor blade are shown in Figure 6 to Figure 8. The figures respectively show the pressure at selected radial positions: r/R=0.500, 0.825 and 0.975 for one main rotor revolution at azimuthal spacing of 30^o. Experimental values are represented by symbols while the numerical results are represented by solid curves. The pressure sensors were distributed on three blades. For each blade a different colour is used in the figures. The experimental data shown were averaged over a comparably large number of rotor revolutions of that used for the fuselage sensors.

Qualitatively, the computations captured the pressure pattern well over the whole revolution for the three radial locations. There is a slight overestimation of the computed pressure on the suction side for the advancing range up to $\Psi=150^o$ at r/R=0.5. The agreement improves for a small part of the retreating range (up to $\Psi=210^o$) then a deviation from the experiment is observed again for the rest of the revolution. Comparison of the computed and measured pressure patterns in the remaining azimuthal position indicates a slightly higher effective angle of attack experienced in the computations.

At r/R=0.825, Figure 7, the computational results are very close to the experimental data. Apart from discrepancy on the suction side in the range $\Psi=30^o$ to 90^o, and at $\Psi=180^o$, the numerical results match the measurements very good.

Similarly good agreement is found in Figure 8 for the radial location r/R=0.975. Some discrepancy is observed at $\Psi=90^o$, 120^o and 180^o. However, at some of these locations ($\Psi=90^o$ and 120^o), the overshoot observed between CFD and experiment is limited mainly to a single sensor.

Tail rotor pressures at the radial locations r/R=0.8 and 0.97 are presented respectively in Figure 9 and Figure 10. Similar to the main rotor data, sectional pressure plots are shown with azimuthal spacing of 30^o. Solid curves refer to numerical results and symbols refer to measured data. As mentioned earlier, the computations were performed ahead of the computations according to prescribed test matrix. In the experiment, different tail rotor commands were applied than the experimental

ones. The numerical data are nevertheless close to the experimental measurements at several azimuthal positions. The deviation is most obvious in the range between Ψ_{tr}=60° and 120°. Beyond this location and up to Ψ_{tr}=180°, the agreement is enhanced. In the retreating range, Ψ_{tr}=180°-360°, the effective dynamic pressure diminishes causing a collapse of the sectional pressure curves, bringing the numerical and experimental value closer to each other. A clear statement on the quality of results is therefore hard to make. However, the agreement looks very reasonable for both radial locations.

Figure 11 compares PIV and CFD velocity fields immediately downstream of the exhaust pipes. The measurements show that the flow around a helicopter is not perfectly 4/Rev periodic as it always assumed. There are minor, but obvious differences in the evolution of the wake between the Ψ=0° and 90° positions. This is seen in the delayed decomposition (or early fusion) of vortex (A) behind the left (as shown in the figure) exhaust pipe. The same can be observed for vortex group (B). At Ψ=90° the decomposition process of vortex group (C) is similar to that at 0°, but seems to be slightly ahead in phase. The outer vortex is almost completely disintegrated and starts to interact with the upper vortex.

A different streamline pattern is found in the computations. Two large vortices are observed on the retreating (right in the figure) side. Similar to the experiment, the 4/Rev periodicity is not complete as can be seen in the deviation in sizes and positions of vortices between Ψ=0° and 90° plots. The two corner vortices (D) detected in the measurements were not reproduced by in the computations. This can be consequence of the geometrical difference s mentioned previously, and might also be due to insufficient grid resolution in this region.

6. CONCLUSIONS

Results of blind, time-accurate RANS simulation of a complete helicopter configuration under cruise conditions were examined by comparison with experimental data. Weak fluid-structure coupling was iteratively applied in the computations to trim the main rotor to generate the same propulsive, lateral and vertical force as in the experiment.

Fluid-structure-flight mechanics coupling proved to be an essential approach for accurate prediction of the pressure on the rotor. The agreement between computed and measured pressure on the main rotor has improved significantly compared to the results presented in [1], especially in the advancing range (60°-180°).

Good agreement could also be found on the front upper part of the fuselage in terms of phase and magnitude. On the tail boom and tail gate evident discrepancy was observed most probably caused by geometrical differences between the wind tunnel and the computational models.

Computed tail rotor pressure signals match the experimental measurements well. The observed deviation is likely caused by application of different rotor commands.

The post test computations, which are currently being performed, simulate the actual geometry tested in the wind tunnel. Final remark on the quality of prediction can be only made after the evaluation of the post test calculations.

ACKNOWLEDGEMENT

This investigation was carried out as a part of the European Union Specific Targeted Research Project GOAHEAD (GROWTH Contract Number AST4-CT-2005-516074). The author would like to thank the European Union for financial support.

REFRENCES

[1] Khier, W., Schwarz, T., Raddatz, J., Time Accurate Simlation Of The Flow Around The Complete BO105 Wind Tunnel Model, *Proceedings of the 31st European Rotor Craft Forum, 13-15th* Sept. 2005, Florence, Italy.

[2] Pahlke, K., Van der Wall, B., Calculation of multi-bladed rotors in high speed forward flight with weak fluid-structure coupling. *Proceedings of the 27th European Rotorcraft Forum, Moscow, Russia,* September 2001.

[3] Langer, H.-J., Dieterich, O., Oerlemans, S., Schneider, O., Van der Wall, B., Yin, J., The EU HeliNOVI Project -Wind Tunnel Investigations for Noise and Vibration Reduction. *Proceedings of the 31st European Rotorcraft Forum*, 13-15 September 2005, Florence, Italy.

[4] Yin, J., Van der Wall, B., Oerlemans, S., et al.,

Representative Test results from HeliNOVI Aeroacoustic Main Rotor/Tail Rotor/Fuselage Test in DNW. *Proceedings of the 31st European Rotorcraft Forum*, 13-15 September 2005, Florence, Italy.

[5] Deutsches Zentrum für Luft- und Raumfahrt e.V. DLR, Generation of advanced helicopter experimental aerodynamic database for CFD code validation – GOAHEAD – Contract Nr. 516074: Annex I – Description of Work, November 2005.

[6] Pahlke, K., The GOAHEAD project, *Proceedings of the 33rd European Rotorcraft Forum*, Kazan, Russia, September 2007.

[7] Van der Wall, B., Global Model Data Processing and Analysis. GoAhead document number: GOAHEAD / WP4 / DLR / D4.2.10

[8] Boelens, O.J., *et. al.*, The blind-test activity of the GOAHEAD project. *Proceedings of the 33rd European Rotorcraft Forum, Kazan, Russia,* September 2007.

[9] Khier, W., Dietz, M., Schwarz, T., and Wagner, S., Trimmed CFD Simulation of a Complete Helicopter Configuration*, Proceedings of the 33rd European Rotorcraft Forum, Kazan, Russia,* September 2007.

[10] Kroll, N., Rossow, C.-C., Becker, K., Thiele, F., The MEGAFLOW project, Aerospace, Science and Technology, Vol. 4, pp. 223-237, 2000.

[11] `Kroll, N., Eisfeld, B., Bleecke, H.M., The Navier-Stokes Code FLOWer. Volume 71 of Notes on Numerical Fluid Mechanics, pp. 58-71. Vieweg, Braunschweig, 1999.

[12] Benoit, B., Dequin, A-M., Kampa, K., Grünhagen, W. v., Basset, P-M., Gimonet, B., HOST: A General Helicopter Simulation Tool for Germany and France. *56th Annual Forum of the American Helicopter Society, Virginia Beach, Virginia,* May 2000.

[13] Baldwin, B. S., Lomax, H., Thin Layeer Approximation and Algebraic Model for Separated Turbulent Flows, 78-0257, 1978.

[14] P. R. Spalart, S. R. Allmaras, A One-Equation Turbulence Model for Aerodynamic Flows, AIAA paper, 92-439, 1992.

[15] Rudnik, R., Untersuchung der Leistungsfähigkeit von Zweigleichungs-Turbulenzmodellen bei Profilumströmungen, Deutsches Zentrum für Luft- und Raumfahrt e.V., FB 97-49

[16] Wilcox, D. C., Reassessment of the Scale-Determining Equation for Advanced Turbulence Models, AIAA Journal, vol. 26, no. 11, November 1988.

[17] Dietz, M., Krämer, E., Wagner, S., Altmikus, A., Weak coupling for active advanced rotors. *Proceedings of the 31st European Rotorcraft Forum, Florence, Italy,* September 2005.

[18] Dietz, M., Khier, W., Wagner, S. and Krämer, E., Numerical simulation of a full helicopter configuration using weak fluid-structure coupling. 46th AIAA Aerospace Sciences Meeting and Exhibit, Reno, Nevada, 7th–10th January 2008, AIAA 2008-401.

[19] Dietz, M., Keßler, M., Krämer, E., Trimmed simulation of a complete helicopter configuration using fluid-structure coupling, to be published in high performance computing in science and engineering 2007, Springer Verlag, 2007.a.

[20] Dietz, M., Simulation der Umströmung von Hubschrauberkonfigurationen unter Berücksichtigung von Strömung-Struktur-Kopplung und Trimmung. Ph.D. Thesis. Institut für Aerodynamik und Gasdynamik, Universität Stuttgart. Stuttgart, Germany, 2009.

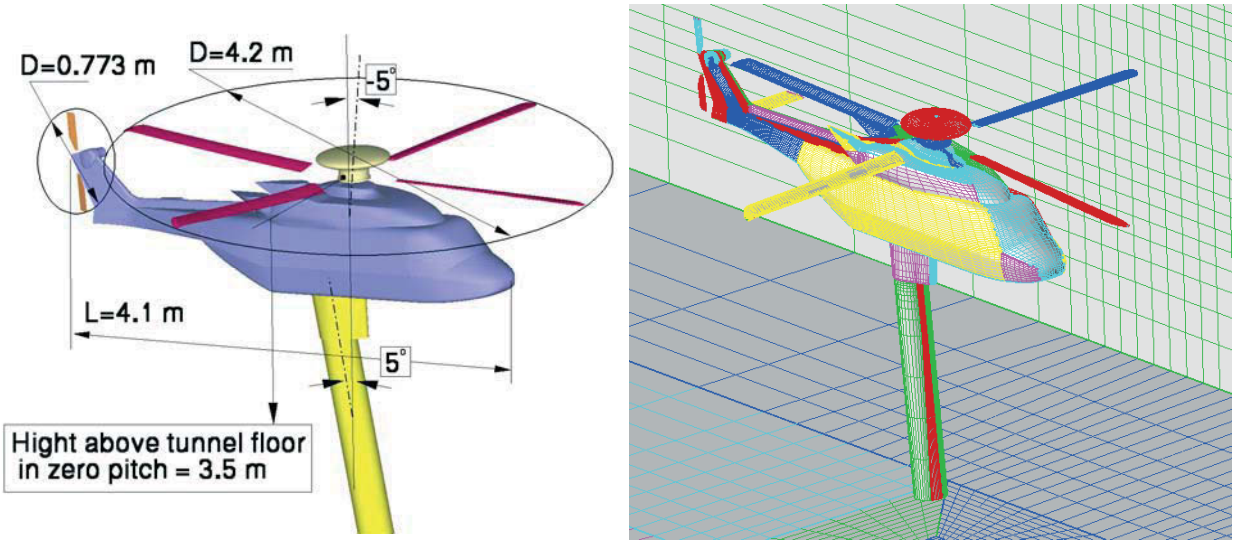

Figure 1: Left: Overview of the computational model showing its main components. Wind tunnel section not shown. Right: Surface grid on the model and wind tunnel walls

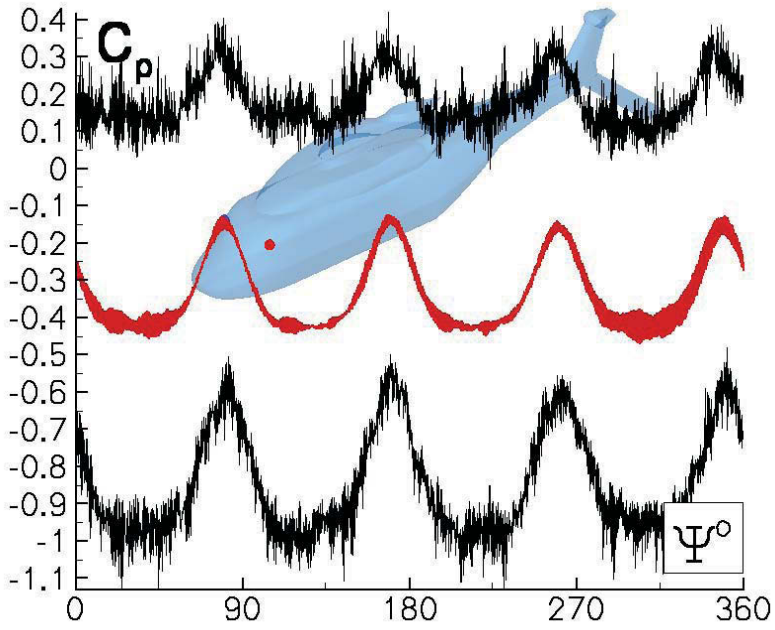

Figure 2: Measured pressure maxima and minima of 130 readings (black curves) over one main rotor revolution. Averaged data shown in red.

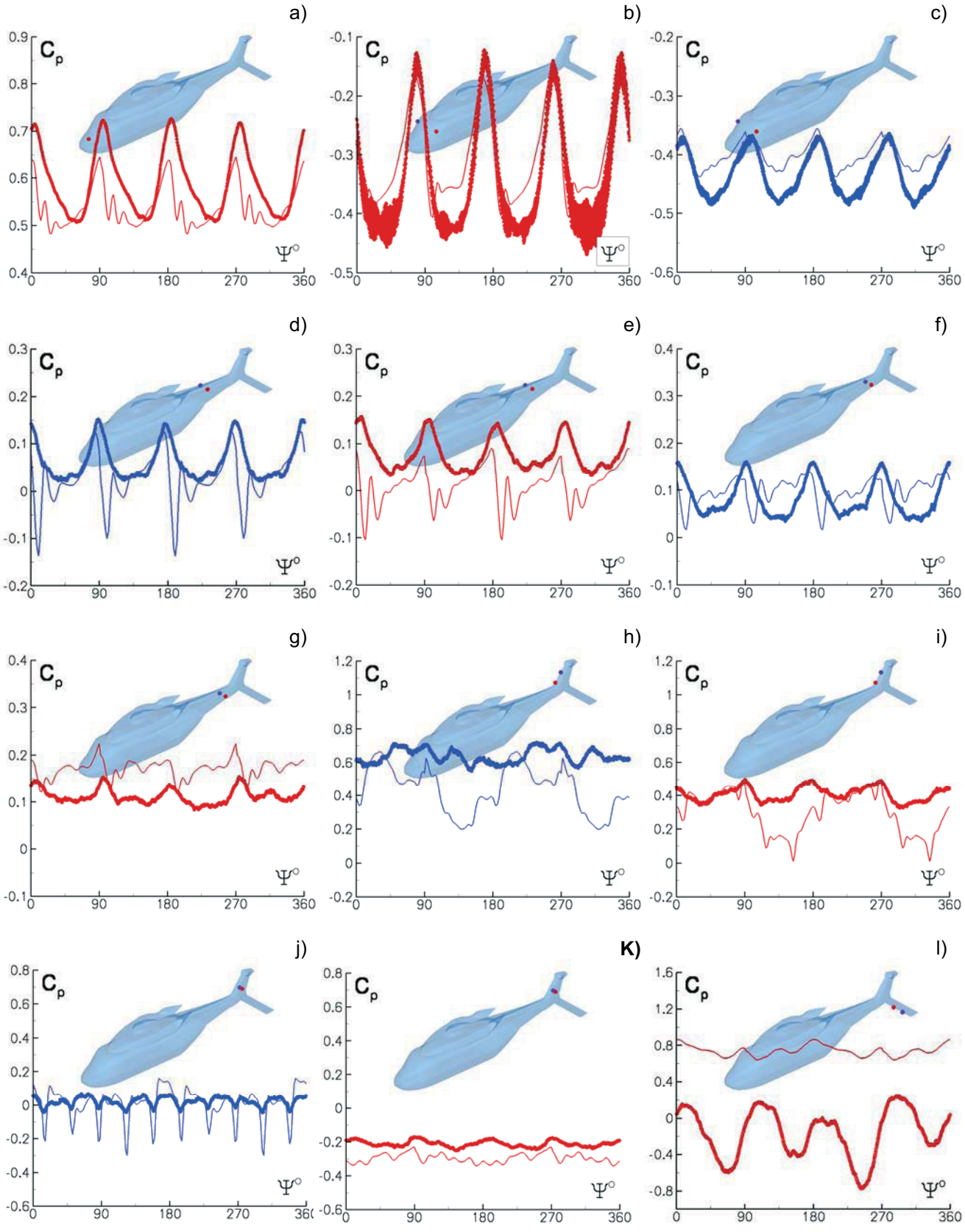

Figure 3: Computed (thin curves) and measured (thick curves) evolution of surface pressure at selected locations on the fuselage.

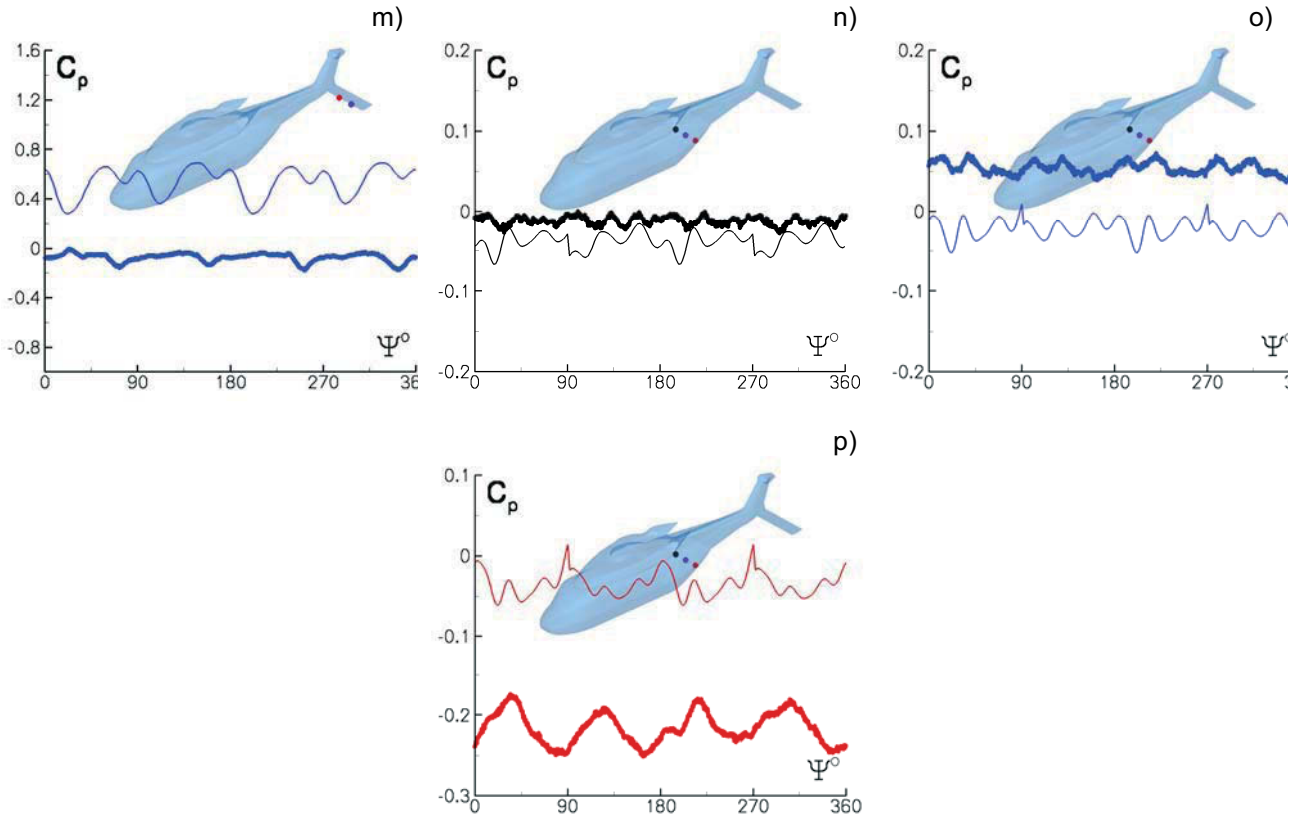

Figure 3 Continued

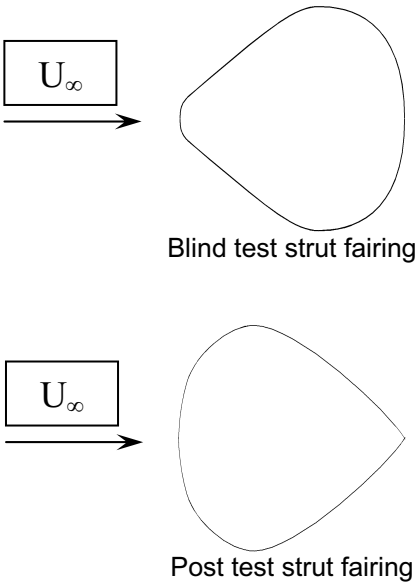

Figure 4: A sketch showing the difference between the blind and post tests strut fairings. Drawing not to scale

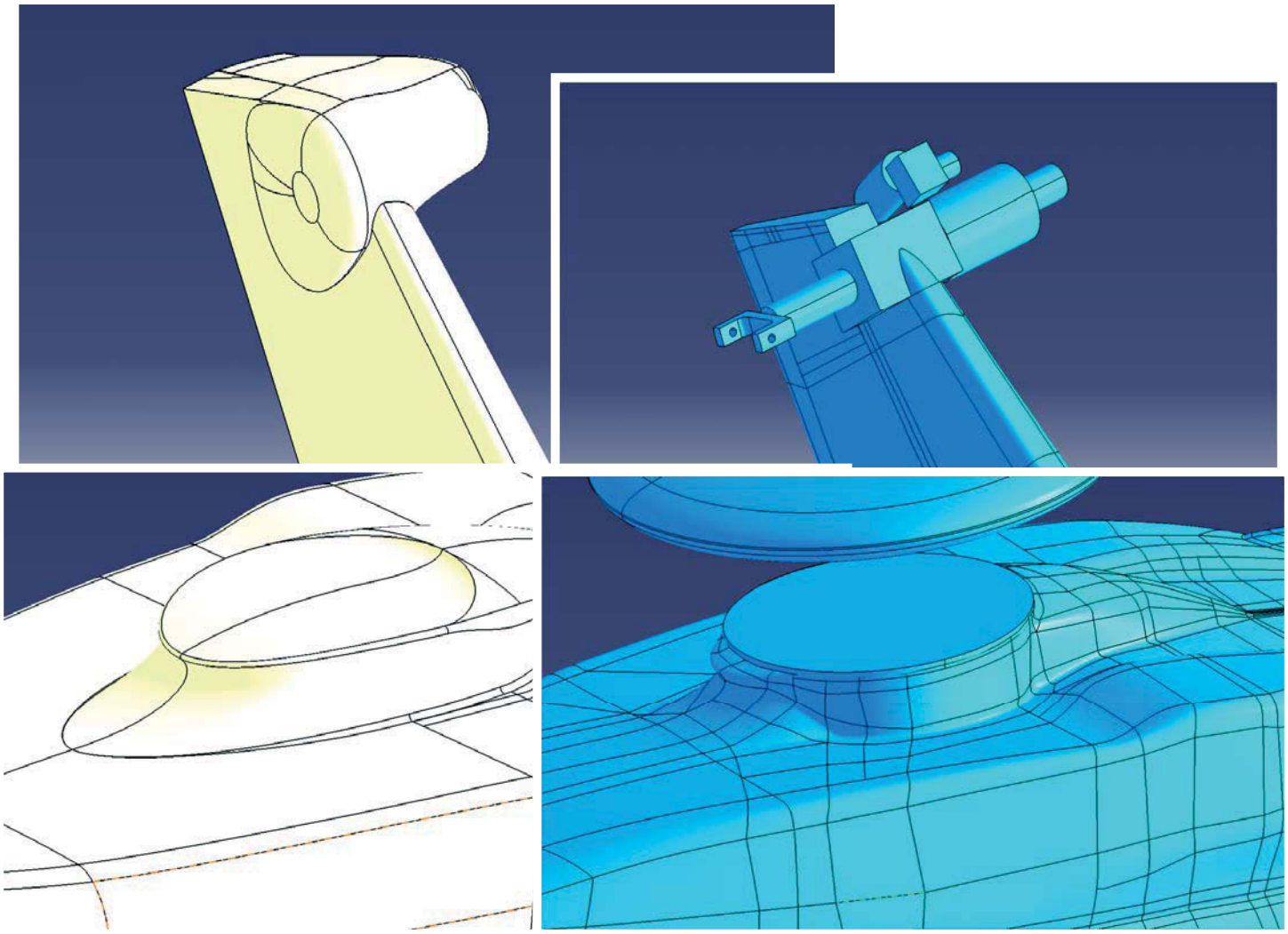

Figure 5: Geometrical differences between the blind test geometry (left) and the wind tunnel model (right)

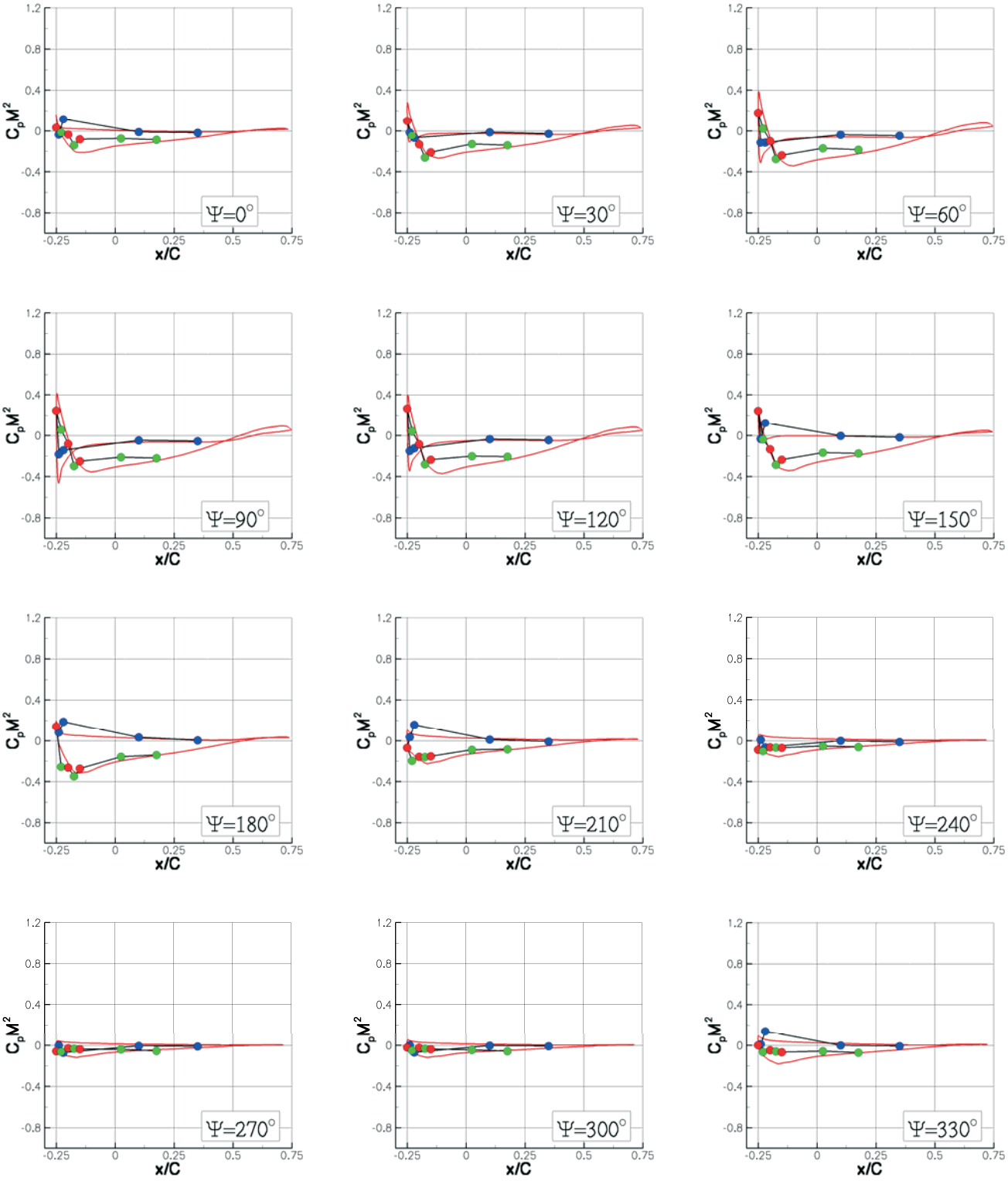

Figure 6: Computed (red curves) and measured (symbols) main rotor sectional pressure at r/R=0.500 at several azimuthal positions. Symbols of different colours belong to different blades.

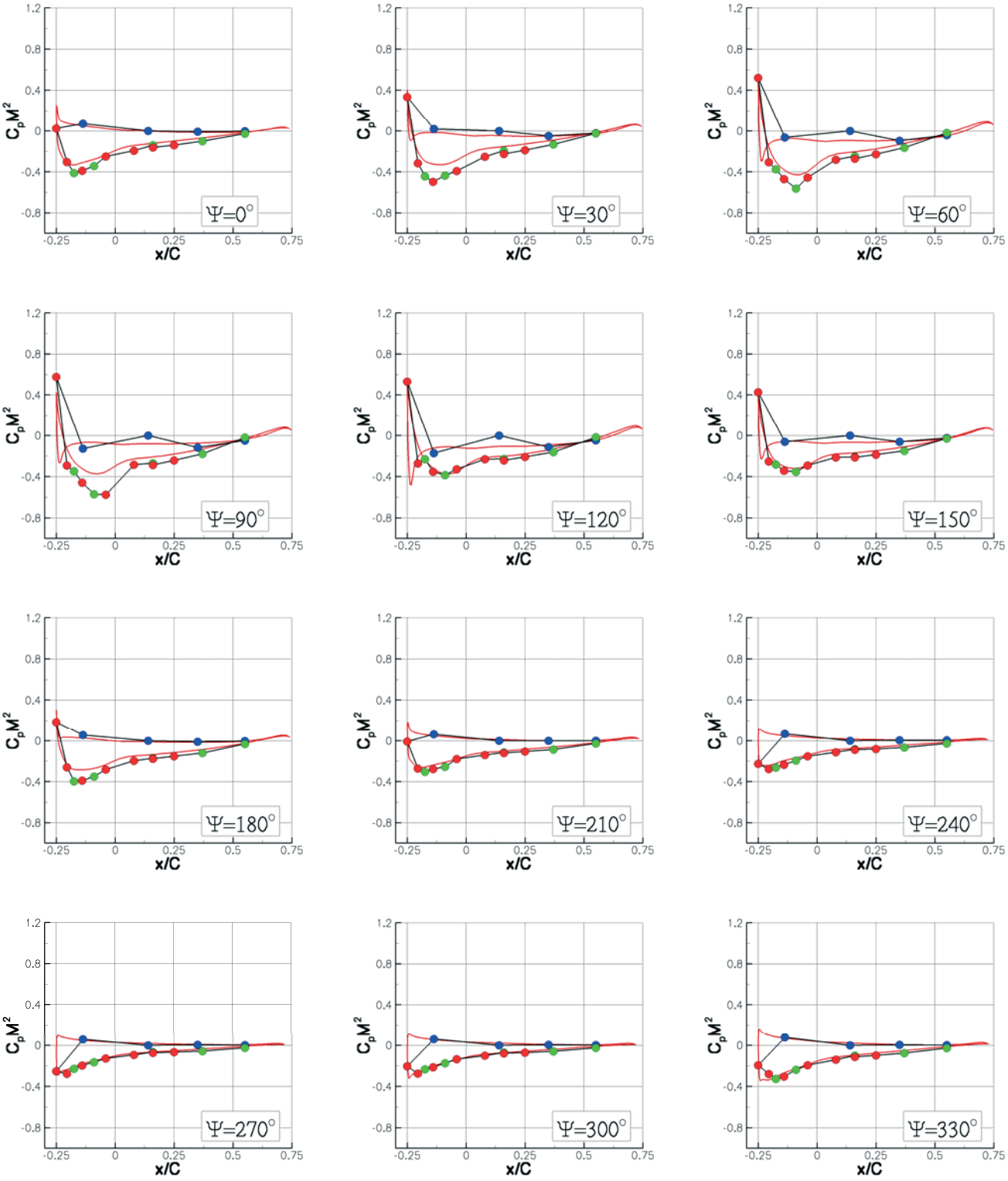

Figure 7: Computed (red curves) and measured (symbols) main rotor sectional pressure at r/R=0.825 at several azimuthal positions. Symbols of different colours belong to different blades.

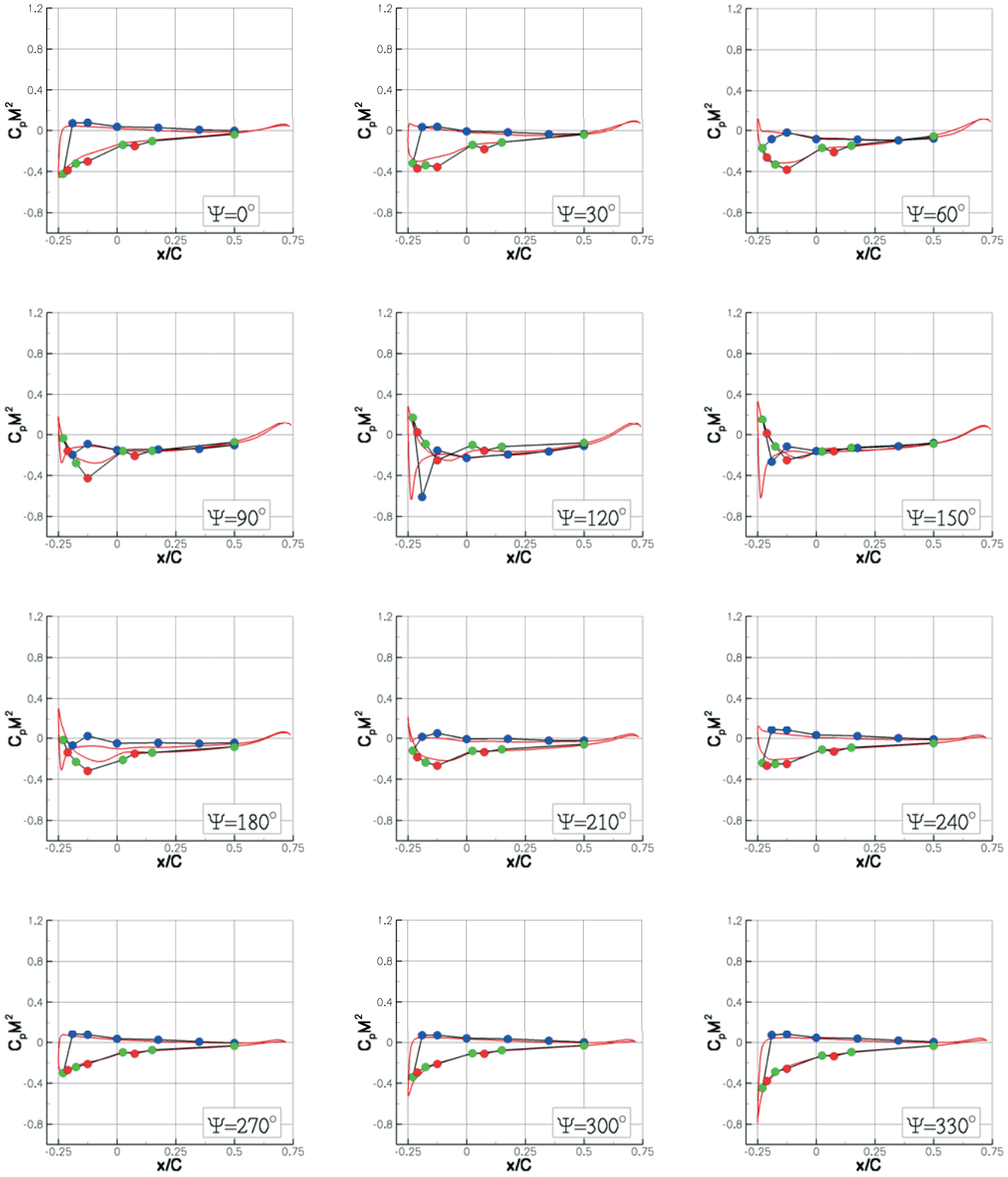

Figure 8: Computed (red curves) and measured (symbols) main rotor sectional pressure at r/R=0.975 at several azimuthal positions. Symbols of different colours belong to different blades.

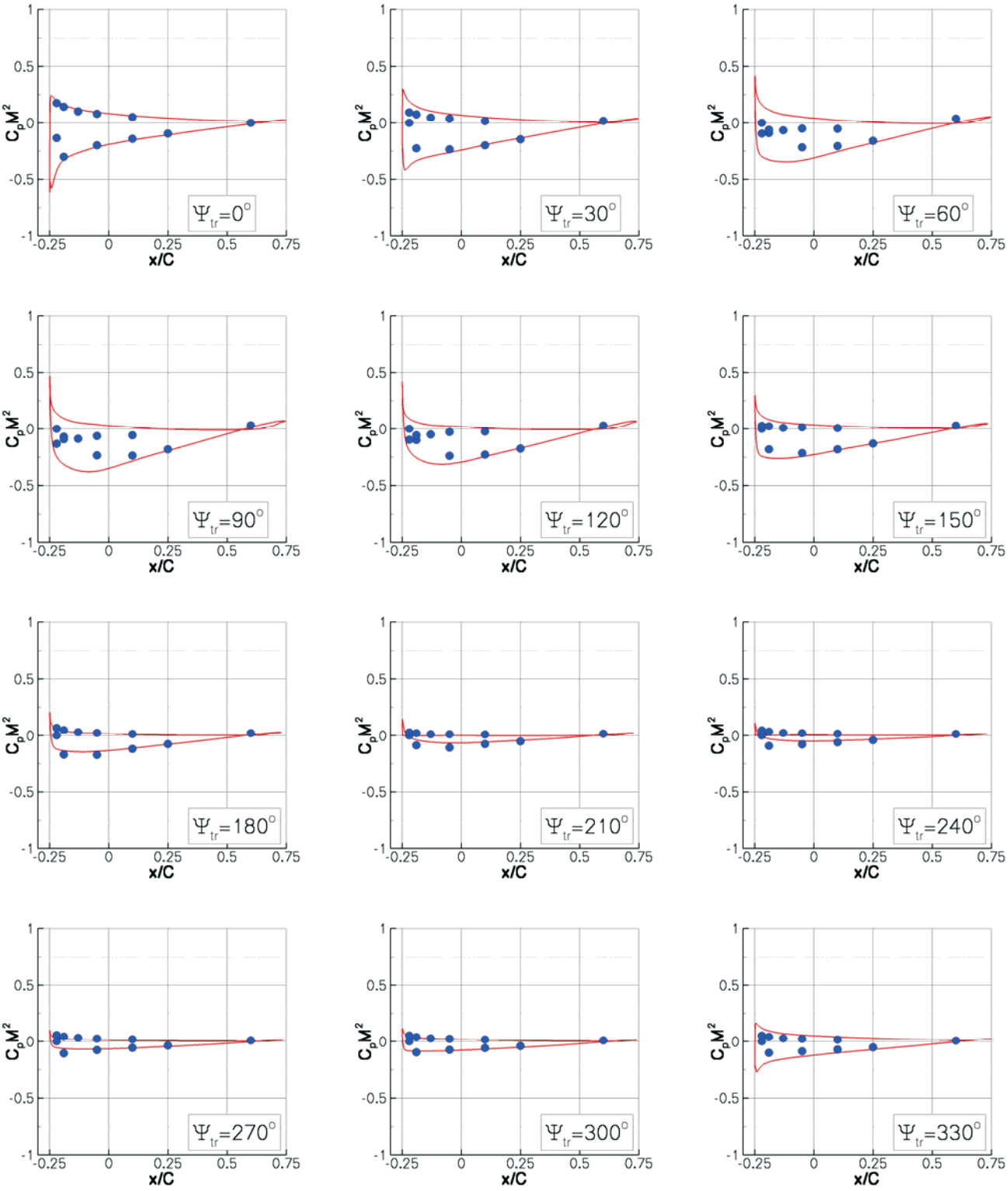

Figure 9: Computed (red curves) and measured (blue symbols) tail rotor sectional pressure at r/R=0.8 at several azimuthal positions.

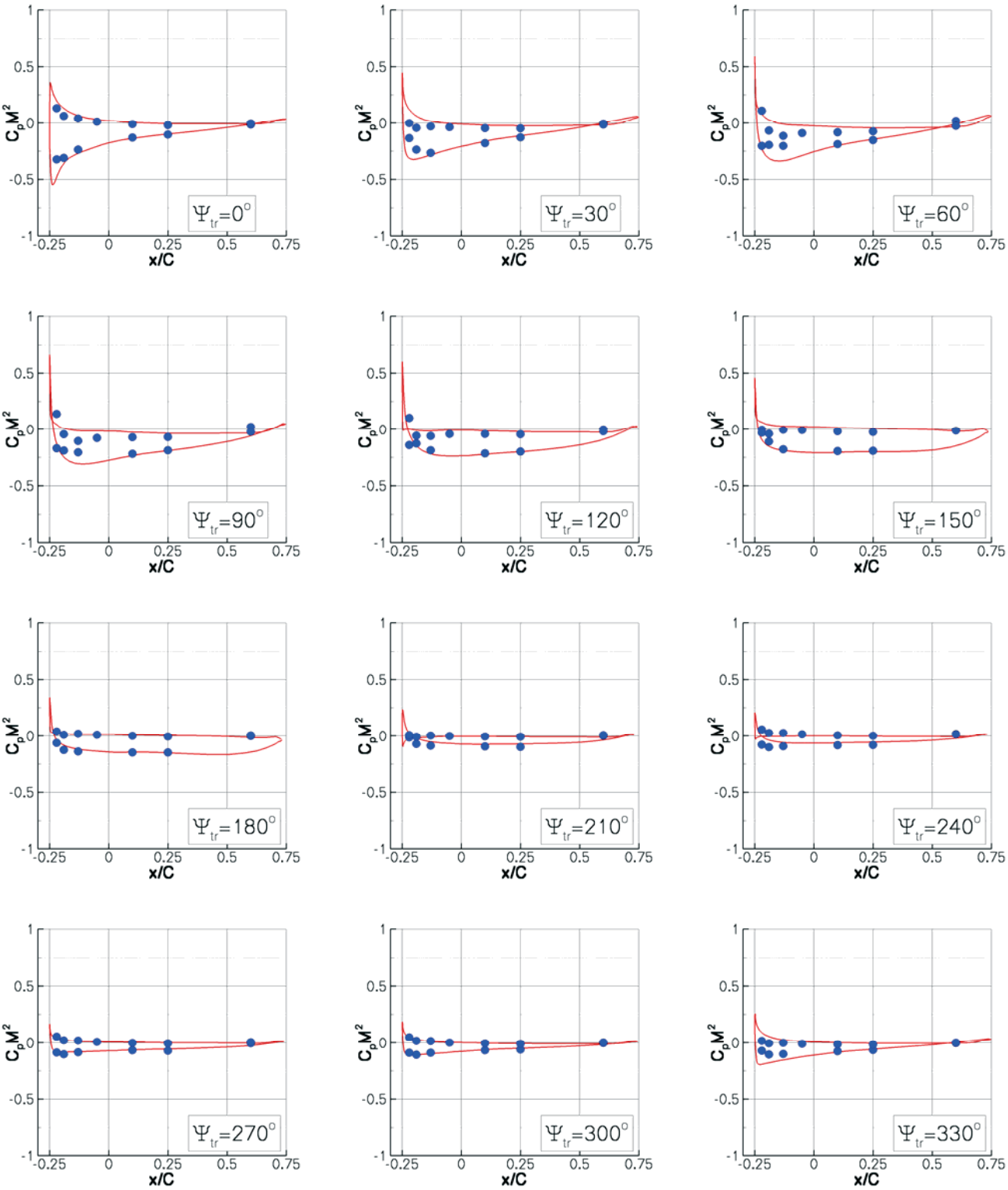

Figure 10: Computed (red curves) and measured (blue symbols) tail rotor sectional pressure at r/R=0.97 at several azimuthal positions.

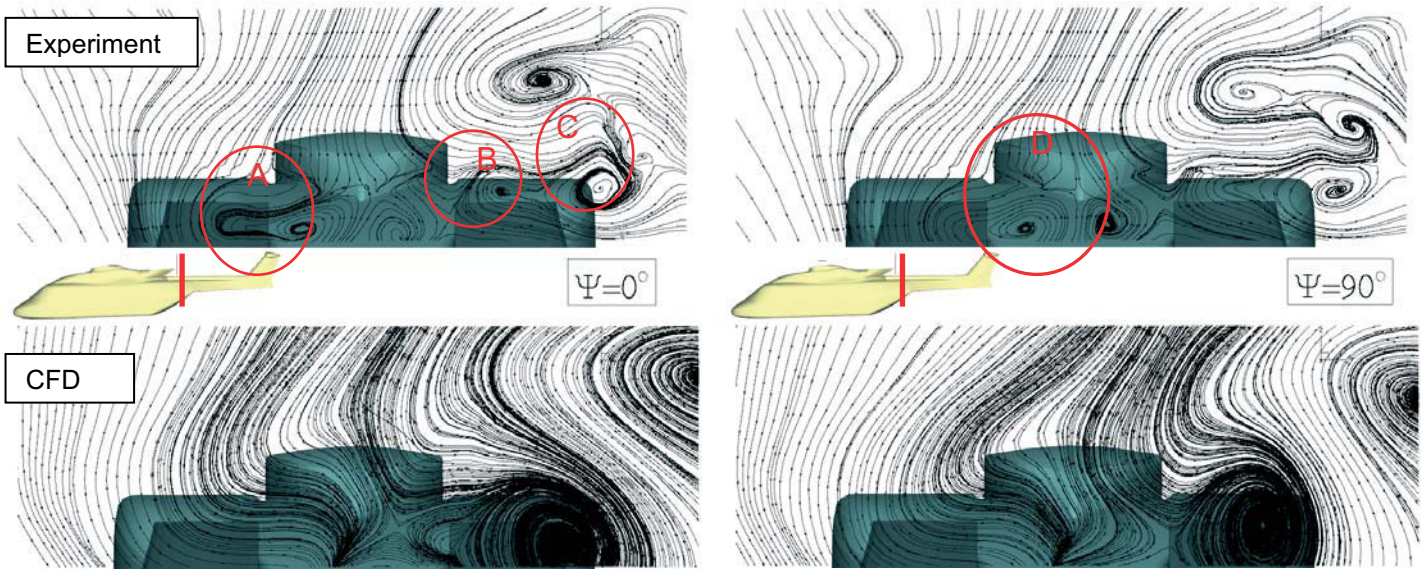

Figure 11: Wake structure (looking upstream) immediately downstream exhaust pipes for $\Psi=0^{o}$ (left) and 90^{o} (right). Upper plots: experiment, Lower plots: CFD